ELSEVIER

Journal of Nuclear Materials 279 (2000) 107–117

journal of nuclear materials

www.elsevier.nl/locate/jnucmat

Delayed hydride cracking in zirconium alloys in a temperature gradient

S. Sagat [a,*], C.K. Chow [b], M.P. Puls [c], C.E. Coleman [a]

[a] *Fuel Channels Division, Materials and Mechanics Branch, AECL Chalk River Laboratories, Chalk River, Ont., Canada K0J 1J0*
[b] *AECL, WL, Pinawa, Man., Canada R0E 1L0*
[c] *AECL, SP, Mississauga, Ont., Canada L5K 1B2*

Received 22 July 1999; accepted 18 October 1999

Abstract

Past theoretical models of delayed hydride cracking in zirconium alloys have assumed a uniform temperature distribution in the material. However, in real components, a temperature gradient may be set up, for example, when a through-wall crack leaks hot, pressurized fluid. Since hydrogen is thermodynamically inclined to diffuse to cold regions, its diffusion to the flaw tip in a thermal gradient will be affected. We have modified the steady-state model of delayed hydride cracking to take account of such a temperature gradient. The new model predicts an increase in the crack velocity in a positive temperature gradient (crack-tip cooler than surroundings) and a reduction in a negative temperature gradient. The model also predicts a shift in the temperature at which cracking ceases if the temperature is attained by heating; this critical temperature increasing in a positive gradient and decreasing in a negative gradient. Experiments have confirmed the trends predicted by the modified model of DHC.

Nomenclature

α	thickness to length ratio of the hydride
$\sigma^{a}_{i,j}$	applied stress tensor
$\varepsilon^{T}_{i,j}$	strain tensor: stress-free (or transformation) strains of α-Zr transformed to hydride
v	Poisson's ratio
$(\overline{w}^{a}_{t})$	interaction energy of the hydride with the applied stress $= -\overline{V}_{H}\sigma^{a}_{i,j}\cdot\varepsilon^{T}_{i,j}$
$(\overline{w}^{inc}_{t})^{eff}$	total effective molal strain energy in an infinite matrix of matrix and hydride precipitate
$\overline{w}^{inc}_{t}$	total molal strain energy in an infinite matrix of matrix and hydride precipitate assuming that there is no plastic deformation in the matrix or hydride
$\overline{w}^{a}_{H}$	molal interaction energy of the local value of the applied stress with the hydrogen in solution
Ω_{Zr}	atomic volume of zirconium
A	constant
B	constant
a_{c}	critical length of the hydride
C_{0}	pre-exponential term in C^{S}_{H}
C_{H}	concentration of hydrogen in solution in zirconium
C^{S}_{H}	concentration of hydrogen in equilibrium with unconstrained hydrides when there is no external stress
D_{H}	diffusion coefficient of hydrogen in zirconium (in the absence of hydrides)
$E_{L,l}$	$= \exp\left\{\frac{(\overline{w}^{inc}_{t})^{eff}_{L,l}+(\overline{w}^{a}_{t})_{L,l}-xQ_{C_H}+x(F)_{L,l}}{xR(T)_{L,l}}\right\}$
F	$= -Q^{*}_{H}-BU\left\{\frac{1}{A}-\frac{T}{A^{2}}\ln\left(\frac{T}{r^{1/2}}\right)\right\}$
$G_{L,l}$	$= \exp\left\{\frac{(\overline{w}^{inc}_{t})^{eff}_{L,l}+(\overline{w}^{a}_{t})_{L,l}-xQ_{C_H}}{xRT_{L,l}}\right\}$
I	$= \int_{l}^{L}\frac{1}{r}\exp\left\{\frac{F-\overline{w}^{a}_{H}+Q_{D_H}}{RT}\right\}dr$
J_{H}	hydrogen flux

* Corresponding author.

0022-3115/00/$ - see front matter
PII: S0022-3115(99)00265-2

L	distance from the nearest hydride (see Fig. 2)
l	the position of maximum stress in the plastic zone in front of the crack
M	$-\left\{\frac{1}{RT}\frac{d\overline{w}^{a}_{H}}{dr}-\frac{Q^{*}_{H}}{RT^{2}}\frac{dT}{dr}\right\}$ (see Eq. (A.2))
N	$\frac{\mathrm{CONST}(1)}{rD_{H}}$ (see Eq. A.2)
N_{H}	atomic density of the hydride
P_{h}	hydrostatic stress
Q_{CH}	activation energy for hydrogen concentration
Q^{*}_{H}	heat of transport of hydrogen in zirconium
r	distance from the crack tip
R	gas constant: 8.314 J mol^{-1} K
T	temperature
T_{C}	critical temperature at which DHC stops
t	time
U	energy
V	crack velocity
V_{0}	crack velocity in the absence of temperature gradient
V_{G}	crack velocity in a temperature gradient
$\overline{V}_{H}$	molal volume of hydrogen in solution
$\overline{V}_{\mathrm{hydride}}$	molal volume of hydride
x	ratio of hydrogen to zirconium atoms in hydride

1. Introduction

Zirconium alloy components can fail by a time-dependent mechanism of cracking if they contain hydrides, sharp flaws and are sufficiently stressed. The mechanism of time-dependent hydride cracking, called delayed hydride cracking (DHC), is based on diffusion of hydrogen to the flaw tip, followed by nucleation, growth, and fracture of the flaw-tip hydride. By repeating these processes, the crack can propagate through the component at a rate that is highly dependent on temperature history, Fig. 1. If the cracking temperature is attained by cooling, the crack velocity follows an Arrhenius relationship. If the cracking temperature is attained by heating, above a critical temperature, T_{C}, cracking is slower than that attained by cooling and eventually stops when the temperature is high enough. Theoretical models of this behaviour assume no temperature gradients throughout the component [1–3]. In real components, a temperature gradient may be set up when a hot component touches a cold one. In CANDU reactors, temperature gradients are set up in pressure tubes when they touch their calandria tubes, or at leakage across a crack face when the pressurized water flashes to steam.

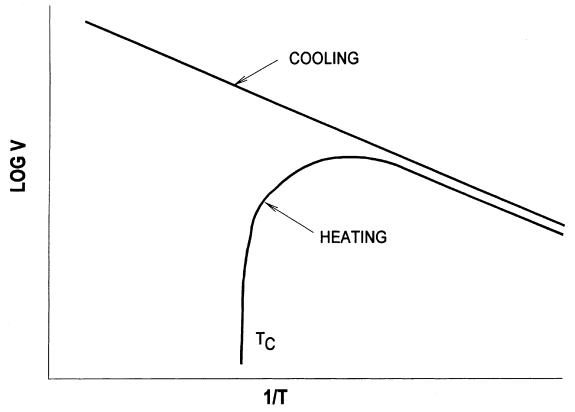

Fig. 1. Schematic diagram of temperature dependence of DHC velocity showing effect of heating and cooling.

In these situations a crack would grow up the temperature gradient, that is, from a cool to a hot region. In graphite-moderated pressure tube reactors, like the N reactor or RBMK reactors, the outside surface of the pressure tube is hotter than the inside surface. A crack forming on the outside surface grows down the temperature gradient.

2. The model

The ground work for modelling DHC in zirconium alloys was laid down by Dutton and Puls [1,2]. Later this model was refined on the basis of the theoretical analysis by Puls [3] of the factors governing hydrogen solubility in stressed and unstressed zirconium alloys. We have extended this model to include the effect of a temperature gradient.

The model is based on the generally accepted mechanism for DHC that consists of the following processes:

1. diffusion of hydrogen to the tip of a flaw,
2. nucleation of a hydride phase at the flaw tip,
3. growth of the hydride phase,
4. fracture of the hydride phase, and
5. repetition of the above processes.

The model describes the first and third processes. Hydride is assumed always to be present in the region around the crack tip and the average crack velocity is assumed to be the steady-state growth of the hydride front, which is assumed for the purposes of the boundary condition in the diffusion solution, in cylindrical geometry, to be located at a radial distance from the crack tip corresponding to the location of the peak in the hydrostatic stress on the crack plane. The actual shape of the hydrided region in front of the crack tip is assumed to be plate-like. The development of some critical condition for fracture of the hydride is assumed, but the

intermittent nature of DHC, which has been demonstrated by experiments, is not modeled.

Assuming the simple, cylindrical geometry with the centre at the crack tip (Fig. 2), a steady-state solution is developed for the diffusion of hydrogen from the source hydrides (assumed located uniformly along the surface of the concentric cylinder of radius L) to the sink hydride (the surface of the concentric cylinder of radius l).

Assuming no heat flux due to a temperature gradient, the main driving force for the hydrogen diffusion from the source, L, to the sink, l, is the chemical potential gradient between L and l set up by the difference in chemical potential of hydrogen in solution equilibrium with the hydrides at L and l. This difference generates two gradient terms in the diffusion equation, one involving the concentration of hydrogen in solution, the other involving the hydrostatic stress, with the latter arising out of a term in the chemical potential giving the differential work done as a result of the interaction of the volume of formation of the hydrogen with the hydrostatic stress. It is the difference in hydrostatic stress at the boundaries at l and L that, initially, is responsible for causing hydrogen to diffuse to the crack tip and form a hydride there, but once formed, generates a concentration gradient between crack tip and bulk hydrides which is the driver for the growth of the crack tip hydride. Adding now an additional driving force to the original hydrogen diffusion equation [1,2] which is due the heat flux generated by a temperature gradient, the cracking rate is assumed to be proportional to the hydrogen flux given by Waisman et al. [4]:

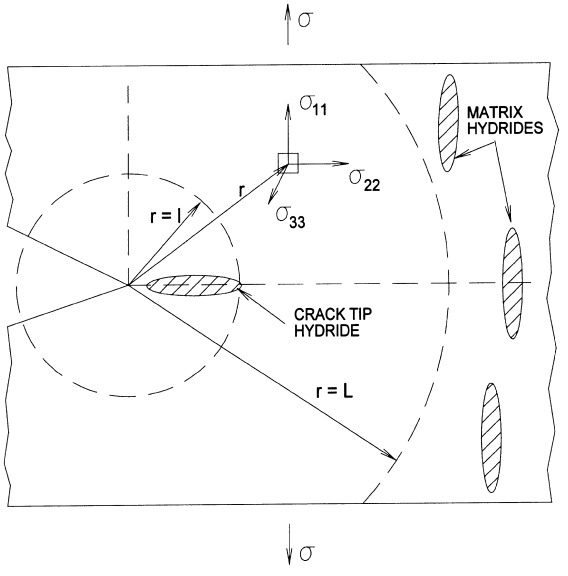

Fig. 2. Schematic diagram of cylindrical crack tip geometry in DHC model.

$$J_{\mathrm{H}} = -\frac{D_{\mathrm{H}}}{\Omega_{\mathrm{Zr}}}\left\{\nabla C_{\mathrm{H}} - \frac{C_{\mathrm{H}}}{RT}\nabla \overline{w}^{\mathrm{a}}_{\mathrm{H}} + \frac{C_{\mathrm{H}}}{RT^2}Q^{*}_{\mathrm{H}}\nabla T\right\}, \tag{1}$$

where D_{H} is the diffusion coefficient of hydrogen in zirconium (in the absence of hydrides), Q^{*}_{H} the heat of transport of hydrogen in zirconium, Ω_{Zr} the atomic volume of zirconium, C_{H} the concentration of hydrogen in solution in zirconium, $\overline{w}^{\mathrm{a}}_{\mathrm{H}}$ the molal interaction energy of the local value of the applied stress with the hydrogen in solution $= p_{\mathrm{h}} \cdot \overline{V}_{\mathrm{H}}$ (ignoring second order terms), p_{h} the hydrostatic stress and $\overline{V}_{\mathrm{H}}$ is the molal volume of hydrogen in solution. In Eq. (1), the first two terms inside the brackets describe the effect of the concentration gradient (of hydrogen in solid solution) and the effect of the stress gradient), respectively, as given by Dutton et al. [2]. The consequences on the crack velocity of the effect of the third term, which expresses the effect of the thermal gradient, is developed in this paper.

The mathematical solution of Eq. (1) is given in the Appendix A and the resulting expression for the crack growth rate is

$$\frac{\mathrm{d}a}{\mathrm{d}t} = \frac{2\pi D_0 C_0}{\Omega_{\mathrm{Zr}}\alpha a_{\mathrm{c}} N_{\mathrm{H}} \int_l^L \frac{1}{r}\exp\left\{\frac{F-\overline{w}^{\mathrm{a}}_{\mathrm{H}}+Q_{D_{\mathrm{H}}}}{RT}\right\}\mathrm{d}r}\{E_L - E_l\}, \tag{2}$$

where

$$E_{L,l} = \exp\left\{\frac{(\overline{w}^{\mathrm{inc}}_t)^{\mathrm{eff}}_{L,l} + (\overline{w}^{\mathrm{a}}_t)_{L,l} - xQ_{C_{\mathrm{H}}} + x(F)_{L,l}}{xR(T)_{L,l}}\right\}, \tag{3}$$

$$F = -Q^{*}_{\mathrm{H}} - BU\left\{\frac{1}{A} - \frac{T}{A^2}\ln\left(\frac{T}{r^{1/2}}\right)\right\}, \tag{4}$$

$$T = A + Br^{0.5}, \tag{5}$$

$$U = \frac{2}{3}\frac{K_I}{(2\pi)^{1/2}}(1+\nu)\overline{V}_{\mathrm{H}}. \tag{6}$$

The values of the parameters used to evaluate Eq. (2) are given in Table 1. Note that whether the factor x should be included in Eq. (3) depends on the definition of the hydride molal volume in the expressions for $\overline{w}^{\mathrm{inc}}_t$ and $\overline{w}^{\mathrm{a}}_t$. Thus if the molal volume is expressed as per mole of hydride, then the factor x should be included and is given by the ratio of hydrogen to zirconium atoms in the hydride, whereas if it is expressed as per mole of H, then it can be omitted, since it is equal to unity. In this paper the former definition is used.

Eq. (5) describes the assumed temperature profile ahead of the crack tip (that is between l and L in Fig. 2). To evaluate how much the shape of the temperature profile affects the results, Eq. (2) can be written in the form

Table 1
Parameters used in the model

Parameter	Numerical value	Reference
D_H	$2.17 \times 10^{-7} \exp\left(\frac{-35\ 100}{RT}\right)$ m^2/s	[5]
C_H^S	$10.2 \exp\left(\frac{-35\ 000}{RT}\right)$ atoms/atom	[6]
Q_{D_H}	35 100 J/mol	[5]
Q_{C_H}	35 000 J/mol	[6]
Q_H^*	25 100 J/mol	[7]
Ω_{Zr}	2.3×10^{-29} m^3/atom	[8]
$V_{hydride}$	16.3×10^{-6} m^3/mol hydride	[8]
σ_{ij}^a σ_{11}^a	400 at L, $3.0\sigma_y$ at l, MPa	[9]
σ_{22}^a	400 at L, $1.8\sigma_y$ at l, MPa	[9]
σ_{33}^a	240 at L, $2.4\sigma_y$ at l, MPa	[9]
ε_{ij}^T $\varepsilon_{11}^T \parallel \langle 0001 \rangle$	0.072	[9]
$\varepsilon_{22}^T \parallel \langle 1\bar{1}00 \rangle$	0.0458	[9]
$\varepsilon_{33}^T \parallel \langle 1\bar{1}20 \rangle$	0.0458	[9]
σ_y	$1088 - 1.02 \cdot T$(K), MPa	[10]
N_H	6.13×10^{28} atom/m^3	[11]
α	0.1	
x	1.66	[8]

$$\frac{da}{dt} = \frac{2\pi D_0 C_0}{\Omega_{Zr} \alpha a_c x N_H} \left\{ G_L \exp\left[\frac{F_L}{RT_L}\right] \Big/ I - G_l \exp\left[\frac{F_l}{RT_l}\right] \Big/ I \right\}, \tag{7}$$

where

$$G_{L,l} = \exp\left\{ \frac{\left(\overline{w}_t^{inc}\right)_{L,l}^{eff} + \left(\overline{w}_t^a\right)_{L,l} - xQ_{C_H}}{xRT_{L,l}} \right\} \tag{8}$$

and

$$I = \int_l^L \frac{1}{r} \exp\left\{ \frac{F - \overline{w}_H^a + Q_{D_H}}{RT} \right\} dr. \tag{9}$$

The terms G_L and G_l depend only on the temperatures T_L and T_l and are independent of the shape of the thermal gradient. Numerical evaluation of Eq. (7) for various T values between 370 and 570 K and for $T_L - T_l$ values between 0 and 20 K, indicate that for each value of T

$$\exp\left(\frac{F_L}{RT_L}\right) \Big/ I \approx \exp\left(\frac{F_l}{RT_l}\right) \Big/ I \tag{10}$$

and that both sides of Eq. (10) are almost independent of $T_L - T_l$. It follows that the shape of the thermal gradient will have a minor effect on the predicted crack growth rates; the main effect comes from the temperature difference, $T_L - T_l$. Thus the model can be used to predict the effects of a thermal gradient whatever the shape of the thermal gradient.

3. Numerical evaluation of the model

3.1. Uniform temperature distribution

To perform a numerical evaluation of the model, as given by Eq. (2), we assume that

1. the crack tip hydrides, ZrH_x, are of the δ phase ($x = 1.66$),
2. the growth of the crack tip hydrides is evaluated at the position of maximum stress and the distance of this position from the crack tip defines the critical hydride length a_c,
3. L is 500 μm [11].

The terminal solid solubility for precipitation (TSSP) was defined by Puls [9] as the cooling TSS

$$\left(C_H^S\right)_{cooling} = C_H^S \exp\left\{ \frac{\overline{w}_t^{inc} + \overline{w}_t^a}{xRT} \right\} \exp\left\{ \frac{\overline{w}_H^a}{RT} \right\}, \tag{11}$$

where $\overline{w}_t^{inc}$ is the total molal strain energy of hydride formed in an infinite matrix assuming that there is no plastic deformation in the matrix or hydride. For a δ-hydride, it is 4912 J/mol hydride [10]. The concentration, C_H^S, is the solubility of hydrogen in equilibrium with unconstrained hydrides. Note that experimentally determined values for C_H^S do not exist, but an approximation is to use the TSS for hydride dissolution (temperature obtained on heating), TSSD.

Because of a 17% volume expansion when the hydride forms in zirconium, there is a hysteresis in TSS due to unrecoverable plastic work. The concentration of hydrogen in solid solution will be greater if the temperature is approached from above (cooling) than if it is approached from below (heating). This is because

$(\overline{w}_t^{\text{inc}})^{\text{eff}}_{\text{cooling}}(L) > (\overline{w}_t^{\text{inc}})^{\text{eff}}_{\text{heating}}(L)$ [3,9]. Because the values of these parameters are not known, they were deduced from the results of DHC tests performed on specimens not subjected to a thermal gradient.

Eq. (2) shows that if $E_L \leqslant E_l$, crack growth cannot occur. It has been shown by experiment on specimens with no thermal gradient [11] that this condition is attained at a certain temperature, T_C, which is different if the temperature is approached by cooling or by heating. Because $(\overline{w}_t^{\text{inc}})^{\text{eff}}_{\text{cooling}}(L) > (\overline{w}_t^{\text{inc}})^{\text{eff}}_{\text{heating}}(L)$, (T_C) on cooling is greater than T_C on heating. T_C on cooling is well above 300°C, while on heating it is about 220°C [11]. The values for $(\overline{w}_t^{\text{inc}})^{\text{eff}}_{\text{cooling}}(L)$ and $(\overline{w}_t^{\text{inc}})^{\text{eff}}_{\text{heating}}(L)$ were obtained by fitting the model to measured crack growth rates obtained after cooling and after heating to the test temperature [11]. The experimental results obtained from the specimens heated to the test temperature were in good agreement with the model predictions for values of $(\overline{w}_t^{\text{inc}})^{\text{eff}}_{\text{heating}}(L)$ between 1750 and 2000 J/mol hydride while for the specimens cooled to the test temperature, values for $(\overline{w}_t^{\text{inc}})^{\text{eff}}_{\text{heating}}(L)$ between 3000 and 4000 J/mol hydride gave best agreement. The range in these values reflects the variability in the crack velocity in the cold-worked Zr–2.5Nb pressure tube material. A more elaborate approach was used by Puls [3] based on using calculated values of the $\overline{w}_t^{\text{inc}}$.

3.2. Model predictions in a temperature gradient

The predicted effects of different positive temperature gradients (the crack tip is cooler than the surrounding metal) on the crack velocity under conditions of cooling to the test temperature as shown in Fig. 3. The model predicts an increase in the crack velocity with increasing temperature gradient. For example, at a crack tip temperature of 500 K, the increase in crack velocity is shown in Table 2, where V_G and V_0 are crack velocities in the presence and absence of temperature gradient, respectively. The main contribution to this increase comes through the increased value of $(E_L - E_l)$. In a uniform temperature, both E_L and E_l are calculated at the same temperature. In a temperature gradient, E_L is calculated for the temperature, T_L, at L (see Fig. 2) which increases the value of E_L. In physical terms this means that the flux of hydrogen to the crack tip increases if the crack tip is cooler than the surrounding material because the hydrogen solubility is lower there, increasing the concentration gradient.

Following heating, the model predicts an increase in the crack velocity in a positive temperature gradient and also an increase in the temperature, T_C, at which cracking stops, as shown in Fig. 4. For example, for a thermal gradient of 20 K/mm, cracking is predicted to stop at 653 K, which is 150 K higher

Table 2
Prediction of crack velocity as a function of positive thermal gradient (Panel A) and negative thermal gradient (Panel B) following cooling to 500 K, where V_G and V_0 are crack velocities with and without temperature gradient, respectively

Thermal gradient (K/mm)	Crack velocity, V_G (m/s)	V_G/V_0
Panel A		
0	2.25×10^{-8}	1.0
5	3.07×10^{-8}	1.04
10	3.95×10^{-8}	1.8
20	5.93×10^{-8}	2.6
40	1.08×10^{-7}	4.8
Panel B		
0	2.25×10^{-8}	1.0
−5	1.49×10^{-8}	0.7
−10	7.84×10^{-9}	0.4
−15	1.36×10^{-9}	0.1

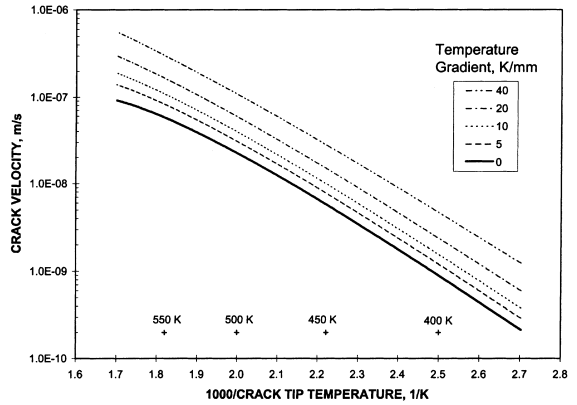

Fig. 3. Model predictions of the effects of positive thermal gradients on the crack velocity following cooling for $(\overline{w}_t^{\text{inc}})^{\text{eff}}_{\text{cooling}}(L) = 3000$ J/mol.

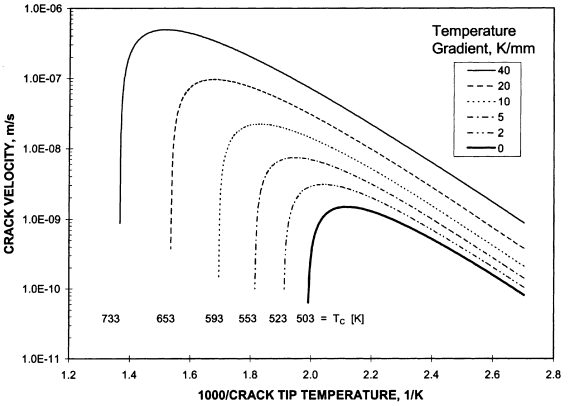

Fig. 4. Model predictions of the effect of positive thermal gradients on the crack velocity following heating for $(\overline{w}_t^{\text{inc}})^{\text{eff}}_{\text{heating}}(L) = 1800$ J/mol.

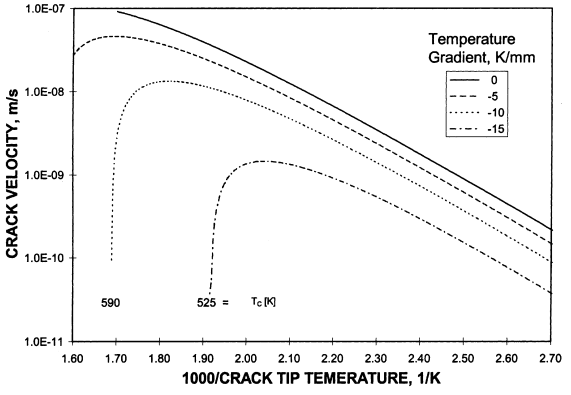

Fig. 5. Model predictions of the effects of negative thermal gradients on the crack velocity following cooling for $(\overline{w}_t^{\text{inc}})^{\text{eff}}_{\text{cooling}}(L) = 3000$ J/mol.

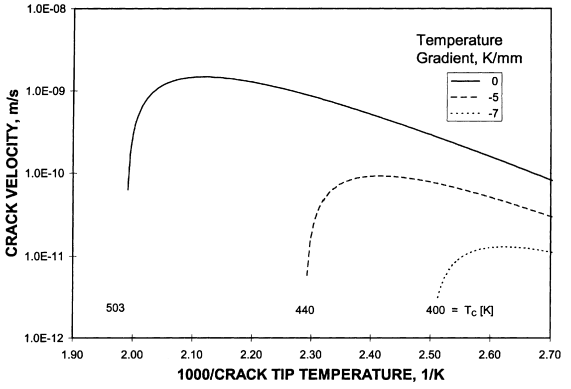

Fig. 6. Model predictions of the effect of negative thermal gradients on the crack velocity following heating for $(\overline{w}_t^{\text{inc}})^{\text{eff}}_{\text{heating}}(L) = 1800$ J/mol.

than the arrest temperature in the absence of the thermal gradient.

If the thermal gradient is negative, that is, the crack tip is hotter than its surroundings, the crack velocity is reduced as shown in Figs. 5 and 6. In addition, the T_C temperature is shifted to lower values depending on the magnitude of the temperature gradient.

4. Confirmation by experiment

Single and double cantilever beam specimens of cold-worked Zr–2.5Nb pressure tube material (2.5–2.6 Nb, 1020–1030 ppm O, 90–110 ppm C and 606–714 ppm Fe), containing up to 0.9 at.% hydrogen, were tested at K_I values of 15–17 MPa $\sqrt{m}$ in various temperature gradients ranging up to 40 K/mm with crack tip temperatures in the range of 420–600 K. In both

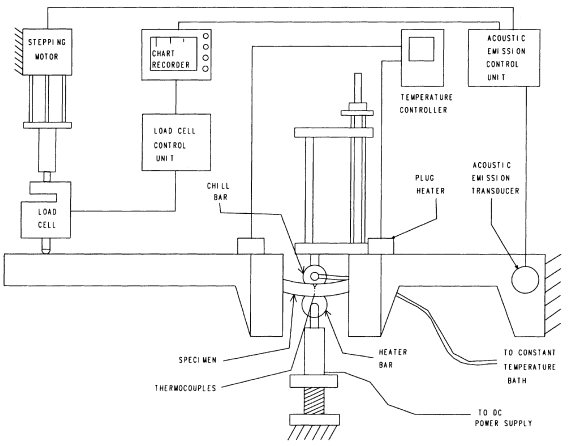

Fig. 7. Experimental set-up for measuring crack velocity, following heating to test temperature, using cantilever beam specimens.

types of specimens the crack-tip zone was cooler than the matrix.

Single cantilever beam specimens were heated by a heater bar attached to the specimen grips, Fig. 7. The positive temperature gradient was superimposed on each specimen by having a chill bar contacting the notch side of the specimen and a heater bar contacting the opposite side of it. The temperature during each test was monitored by five thermocouples spot-welded down one face and two thermocouples down the opposite face of the specimen. The cracking was monitored by acoustic emission and the load was applied by an electric motor drive system [12].

The double cantilever beam specimens (tapered compact toughness specimens) had an electric heater attached to their back and their front was immersed in water, Fig. 8. Starting at the notch, five thermocouples were spot-welded on the specimen at 1 mm intervals.

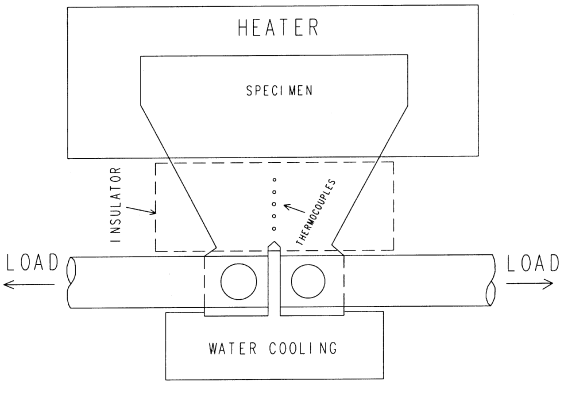

Fig. 8. Experimental set-up for measuring crack velocity using double cantilever beam specimens.

This region was then insulated with silicon rubber. At the beginning of the test, the specimen was heated to a predetermined temperature, loaded to a K_I of about 16 MPa $\sqrt{m}$ and simultaneously the front of the specimen was immersed in water. This reduced the crack tip temperature and produced a temperature gradient in the specimen. Different thermal gradients were achieved by heating the specimen to different temperatures. The crack growth was monitored by DC potential drop.

The single cantilever beam specimens were used to evaluate the effect of a temperature gradient on the T_C temperature when the temperature was approached by heating. In experiments with no temperature gradient, the temperature at which cracking started to slow down, T_C, was about 455 K, and no cracking occurred at temperature >500 K. The T_C temperature was increased by about 90 K if a temperature gradient of 12–25 K/mm was applied. These results are in good agreement with model prediction, Fig. 9.

The double cantilever beam specimens were used to evaluate the effect of the temperature gradient on the crack velocity under optimum conditions for DHC, that is, when the specimens were cooled to the test temperature. The tests were performed in positive thermal gradients between about 7 and 24 K/mm. In each test, the crack was grown for a predetermined length of time. After the test, the specimen was broken open and the crack length measured. Also several isothermal tests (without thermal gradient) were performed. The data agreed with Ambler's expression for the crack velocity [11]:

$$V = 0.686 \exp(-71500/RT), \tag{12}$$

where V is the crack velocity, m/s, $R = 8.314$ J mol^{-1} K and T is the absolute temperature. To analyze the data, this equation was numerically integrated over the range of temperature the crack was grown in each test. A ratio between the computed crack and measured crack velocity was determined for each temperature gradient and compared with the model. Although good numerical agreement with the model prediction was found, Fig. 10, this exact agreement may be fortuitous, in view of the limitations of both model and experiment. Further development and verification of the model is needed for reasons explained in the following.

The first limitation is that the thermal gradient assumed in the model is not exactly the same as it is in the experiment. In the experiment, the crack tip is at a lower temperature than the region in front of it (in the direction of crack growth), but the region behind it is at even lower temperature. This gradient is similar to the actual temperature gradient in leaking pressure tubes or in pressure tubes in contact with calandria tubes, in the direction of the crack growth [13,14]. The model, which was originally developed for DHC in a uniform temperature field, uses a cylindrical symmetry. In a cylindrical geometry the lowest temperature (in the case of a positive gradient) is located at the crack tip and all other points are at progressively higher temperatures with radial distance away from the crack tip. One might expect that having the type of thermal gradient as produced in the experiment could eliminate the effect of the thermal gradient compared to the case of a gradient with cylindrical symmetry since in the region in front of the crack tip the thermal gradient would draw hydrogen to the crack tip, and behind it, it would draw it away to the same extent. That it does not do that, as observed experimentally, is likely due to the hysteresis in the TSS [9] and the fact that when the opposite effects of thermal and hydrostatic stress gradients, are added behind the crack front, the resulting net concentration gradient is incapable of withdrawing hydrogen from hydrides at the crack tip (since the hysteresis in the TSS necessitates a

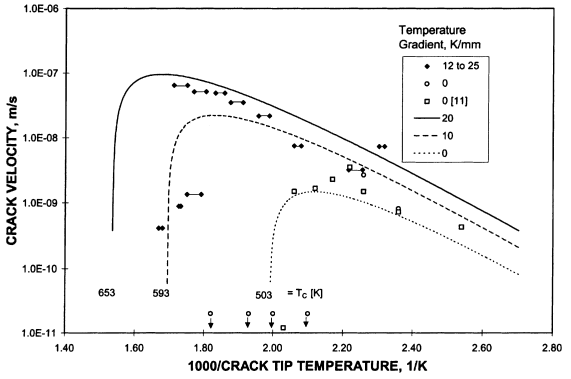

Fig. 9. Comparison between model predictions (curves) and experimental data in tests on cantilever beam specimens with the test temperature approached by heating. The arrows indicate no cracking.

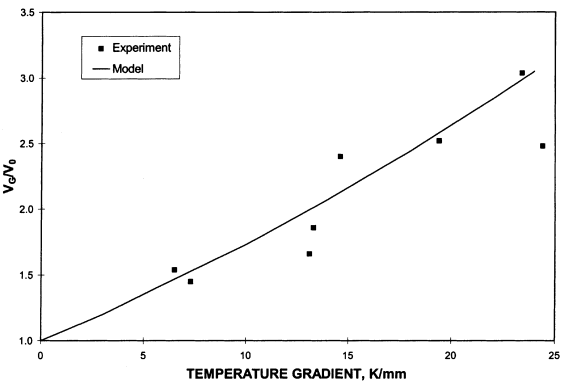

Fig. 10. Ratio of crack velocity measured in thermal gradient, V_G, with integrated velocity in no gradient V_0, as a function of thermal gradient, after cooling to test temperature.

sufficiently large concentration gradient to be set up between source and sink hydrides). Hence the most likely difference on their effect on the DHC velocity of the two types of thermal gradients would be that the thermal gradient used in the experiment should produce a smaller increase in DHC velocity than in predicted by the model.

The second limitation is that the material used in this study happened to have a high temperature dependence as indicated by Eq. (12). The temperature dependence in the DHC model derives primarily from the sum of the activation energies for diffusion and solubility limit contained in the $D_H C_H$ product, which is 70 kJ/mol, Table 1. Secondary effects come from the temperature dependence of the yield stress, which affects the hysteresis in the TSS (this is also affected by the temperature dependence of the elastic constants) and the interaction energy of the applied stress with the hydrogen in solution and the hydride at the crack tip. These secondary effects reduce the total activation energy for DHC growth to about 60 kJ/mol (the slope in Fig. 3). Published activation energies for DHC growth [15] vary from 43 to 72 kJ/mol with the majority of data around 60 kJ/mol. This variability in the temperature dependence is mainly related to the microstructure of the material. Cold-worked Zr–2.5Nb material is a two-phase material consisting of flat, elongated α grains surrounded by thin ligaments of β phase. It is the proportion of the two phases that determines the temperature dependence of DHC growth. However, the current model is only a one-phase (α) model and is not able to model diffusion in a two-phase material. Further development of the model is required before it can be verified against materials with different temperature dependencies of DHC growth.

Experiments with a negative temperature gradient have not been performed.

5. Implications for pressure tubes

Under normal operating conditions in reactor, the temperature gradient in a pressure tube is about 1 K/mm. If a DHC crack is growing through the wall of the tube under these conditions, the crack velocity and T_C will not be measurably affected by such a small gradient. If the pressure tube comes into contact with the calandria tube (the crack growth in this case would be from the contact point on the outside surface of the tube through the tube wall) or a crack penetrates the tube wall and starts to leak, a positive temperature gradient is set up. The temperature gradient arises in the latter because the metal on the crack face is cooled by the pressurized hot water flashes to steam. With a positive temperature gradient, the crack tip will be cooler than the water flashes to steam. With a positive temperature gradient,

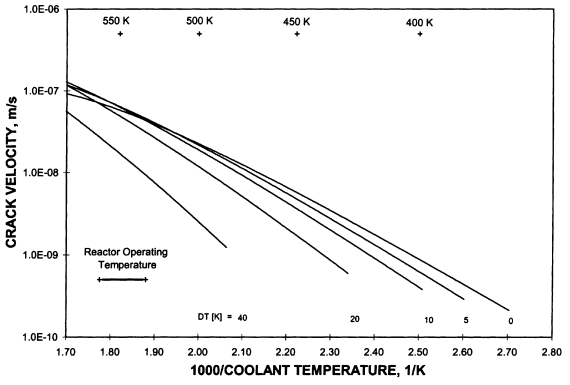

Fig. 11. Model predictions at different thermal gradients, DT, following cooling versus 1/coolant temperature.

the crack tip will be cooler than the water of the heat transport system. Thus, although the gradient increases the crack velocity, the temperature of cracking, and therefore its velocity, are reduced. The effects of the thermal gradient can best be seen if the crack growth rates are plotted as a function of the matrix (coolant) temperature, Fig. 11. Any difference between the crack velocity in the presence of a positive temperature gradient and the crack velocity in the absence of a positive temperature gradient will depend on the size of the gradient and the position of the crack in that gradient. For example, when the pressure tube is operating at 540 K, but has a 10 K/mm gradient through the wall, the outside surface is at 500 K. The crack velocity at 540 K with no gradient is 5.0×10^{-8} m/s while the velocity at 500 K with the gradient 4.0×10^{-8} m/s. Half-way through the tube wall, the crack velocity at 520 K in a 10 K/mm gradient would be 6.2×10^{-8} m/s. Thus, although a temperature gradient increases the crack velocity, the net effect is small because the crack tip temperature is reduced. If the thermal gradient is large

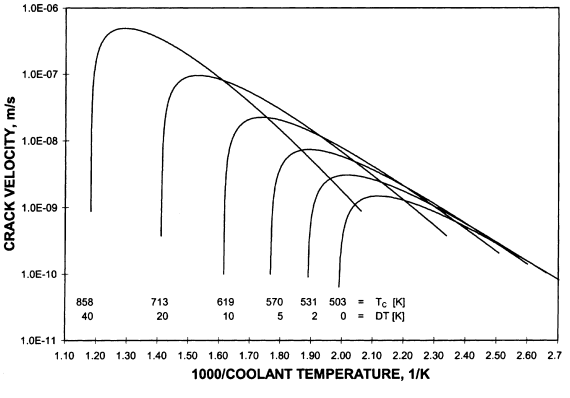

Fig. 12. Model predictions at different thermal gradients, DT, following heating versus 1/coolant temperature.

(>20 K/mm), the crack velocity for a given coolant temperature is reduced because the lower temperature at the crack tip overrides the effect of the thermal gradient.

The shift in T_C to a higher temperature by a temperature gradient has important implications because no credit can be taken for possible crack arrest when approaching the hold temperature from lower temperatures. A temperature gradient of 10 K/mm shifts T_C to 619 K, Fig. 12. Thus the shift of T_C to a higher temperature and the reduction of the temperature of the crack tip in a leaking crack, combine to negate any benefit from approaching the hold temperature from below. The experimental support for this conclusion comes from tests on full-sized rolled joints performed in the Chalk River Active Crack Leak Evaluation (CRACLE) facility [16,17] in which leaking cracks continued to grow with a loop water temperature of 550 K that had been attained by heating.

6. Conclusions

The mathematical model of the effect of a temperature gradient on DHC has been developed and partially confirmed by experiment with the following conclusions:

1. A positive temperature gradient increases the velocity of DHC.
2. A positive temperature gradient increases the critical temperature, T_C, at which cracking stops if the temperature is attained by heating.

Acknowledgements

We would like to acknowledge the contribution by J.F.R. Ambler who developed the theoretical model before he died. We are grateful to D.E. Foote and R.B. Ellis for designing the experimental set-up and for assistance with the experiments. Funding for this work was obtained from the CANDU Owners' Group under Work Package 3125.

Appendix A

Based on the assumption that both stress and temperature at any point depend only on the distance from the crack tip, Eq. (1) can be written in scalar notation as

$$J_H = \frac{-D_H}{\Omega_{Zr}}\left\{\frac{dC_H}{dr} - \frac{C_H}{RT}\frac{d\overline{w}_H^a}{dr} + \frac{C_H Q_H^*}{RT^2}\frac{dT}{dr}\right\}. \tag{A.1}$$

Under steady state conditions

$$\frac{dC_H}{dt} = \nabla \cdot J_H = 0,$$

$$\nabla \cdot J_H = \frac{1}{r}\frac{d}{dr}\left\{rD_H\left(\frac{dC_H}{dr} - \frac{C_H}{RT}\frac{d\overline{w}_H^a}{dr} + \frac{C_H Q_H^*}{RT^2}\frac{dT}{dr}\right)\right\} = 0.$$

Integrating once

$$\frac{dC_H}{dr} - C_H\left\{\frac{1}{RT}\frac{d\overline{w}_H^a}{dr} - \frac{Q_H^*}{RT^2}\frac{dT}{dr}\right\} = \frac{\mathrm{CONST}(1)}{rD_H}. \tag{A.2}$$

From Eqs. (A.1) and (A.2) it follows that

$$J_H = -\frac{\mathrm{CONST}(1)}{\Omega_{Zr} r}. \tag{A.3}$$

Eq. (A.2) is a linear, first order differential equation of the form

$$\frac{dC_H}{dr} + MC_H = N,$$

where M and N are independent of C_H, but not of r. The solution of the equation is

$$C_H = \exp -\left[\int M dr\left\{\exp\left(\int M\,dr\right)N dr + \mathrm{CONST}(2)\right\}\right],$$

which yields, from Eq. (A.2),

$$C_H = \exp -\left[\int M dr\left\{\mathrm{CONST}(1)\int \exp\left(\int M dr\right)\frac{1}{rD_H}dr + \mathrm{CONST}(2)\right\}\right]. \tag{A.4}$$

Using the boundary hydrogen concentrations of $(C_H)_L$ and $(C_H)_l$ and solving for CONST(1) gives

$$\mathrm{CONST}(1) = \frac{((C_H)_L/\exp - \int_0^L M dr) - ((C_H)_l/\exp - \int_0^l M dr)}{\int_l^L \exp(\int M dr)(1/rD_H)dr}. \tag{A.5}$$

From Eq. (A.2)

$$\int M dr = \frac{Q_H^*}{R}\int \frac{1}{T^2}\frac{dT}{dr}dr - \frac{1}{R}\int \frac{1}{T}\frac{d\overline{w}_H^a}{dr}dr, = \frac{-Q_H^*}{RT} - \frac{1}{R}\int \frac{1}{T}\frac{d\overline{w}_H^a}{dr}dr. \tag{A.6}$$

The problem is reduced to solving the term $\int(1/T)(d\overline{w}_H^a/dr)\,dr$ and to do this it has been necessary to assume a temperature distance relationship of the form

$$T = A + Br^{0.5}. \tag{A.7}$$

This relationship fits the thermal gradients predicted by solutions to finite element models of leaking cracks [8]. Since $\overline{w}_H^a = p_h\,\overline{V}_H$ where p_h is the hydrostatic stress and

$\overline{V}_{\mathrm{H}}$ is the partial molal volume of hydrogen in α zirconium, from linear elastic fracture mechanics

$$\overline{w}^{\mathrm{a}}_{\mathrm{H}} = \frac{2K_1}{3(2\pi r)^{0.5}}(1+v)\overline{V}_{\mathrm{H}} = Ur^{-0.5}. \tag{A.8}$$

The term $\int (1/T)(\mathrm{d}\overline{w}^{\mathrm{a}}_{\mathrm{H}}/\mathrm{d}r)$ in Eq. (A.6) can be written as

$$\int \frac{1}{T}\frac{\mathrm{d}\overline{w}^{\mathrm{a}}_{\mathrm{H}}}{\mathrm{d}r}\mathrm{d}r = \frac{\overline{w}^{\mathrm{a}}_{\mathrm{H}}}{T} + \int \frac{\overline{w}^{\mathrm{a}}_{\mathrm{H}}}{T^2}\frac{\mathrm{d}T}{\mathrm{d}r}\mathrm{d}r. \tag{A.9}$$

From Eqs. (A.7)–(A.9) it follows that

$$\int \frac{1}{T}\frac{\mathrm{d}\overline{w}^{\mathrm{a}}_{\mathrm{H}}}{\mathrm{d}r}\mathrm{d}r = \frac{\overline{w}^{\mathrm{a}}_{\mathrm{H}}}{T} + \frac{BU}{2}\int \frac{\mathrm{d}r}{r(A+Br^{0.5})^2}\mathrm{d}r. \tag{A.10}$$

By making the substitutions, $Z = r^{0.5}$, $Z^2 = r$ and $2Z\mathrm{d}Z = \mathrm{d}r$, the integral in Eq. (A.10) becomes a standard form which when solved gives

$$\int \frac{1}{T}\frac{\mathrm{d}\overline{w}^{\mathrm{a}}_{\mathrm{H}}}{\mathrm{d}r}\mathrm{d}r = \frac{\overline{w}^{\mathrm{a}}_{\mathrm{H}}}{T} + BU\left\{\frac{1}{AT} - \frac{1}{A^2}\ln\left(\frac{T}{r^{0.5}}\right)\right\}. \tag{A.11}$$

From Eqs. (A.6) and (A.11):

$$\int M\mathrm{d}r = \frac{-Q^*_{\mathrm{H}}}{RT} - \frac{\overline{w}^{\mathrm{a}}_{\mathrm{H}}}{RT} - \frac{BU}{R}\left\{\frac{1}{AT} - \frac{1}{A^2}\ln\left(\frac{T}{r^{0.5}}\right)\right\}.$$

Let

$$F = -Q^*_{\mathrm{H}} - BU\left\{\frac{1}{A} - \frac{T}{A^2}\ln\left(\frac{T}{r^{0.5}}\right)\right\},$$

$$\int M\,\mathrm{d}r = -\frac{\overline{w}^{\mathrm{a}}_{\mathrm{H}}}{RT} + \frac{F}{RT}. \tag{A.12}$$

From Eqs. (A.3), (A.5) and (A.12) and using the relationship

$$D_{\mathrm{H}} = D_0 \exp\frac{-Q_{D_{\mathrm{H}}}}{RT},$$

it follows that

$$J_{\mathrm{H}} = -\frac{D_0}{r\Omega_{zr}\int_l^L \frac{1}{r}\exp\left(\frac{F-\overline{w}^{\mathrm{a}}_{\mathrm{H}}+Q_{D_{\mathrm{H}}}}{RT}\right)\mathrm{d}r} \left\{\frac{(C_{\mathrm{H}})_L}{\exp\left[\frac{(\overline{w}^{\mathrm{a}}_{\mathrm{H}})_L - F_L}{RT_L}\right]} - \frac{(C_{\mathrm{H}})_l}{\exp\left[\frac{(\overline{w}^{\mathrm{a}}_{\mathrm{H}})_l - F_l}{RT_l}\right]}\right\}. \tag{A.13}$$

Since stress and temperature depend only on the distance r from the crack tip, the rate of diffusion of hydrogen atoms into the cylinder of radius r per unit distance along the cylinder axis is

$$\frac{\mathrm{d}N}{\mathrm{d}t} = -2\pi r J_{\mathrm{H}}.$$

Equating the rate of growth of a crack by DHC, $\mathrm{d}a/\mathrm{d}t$, to the rate of growth of the crack tip hydride

$$\frac{\mathrm{d}a}{\mathrm{d}t} = \frac{-2\pi r J_{\mathrm{H}}}{\alpha a_{\mathrm{c}} N_{\mathrm{H}}}, \tag{A.14}$$

where α is the thickness to length ratio of the hydride, a_{c} the critical length of the hydride and N_{H} is the atomic density of the δ-hydride. To evaluate Eq. (A.14), it is necessary to define expressions for $(C_{\mathrm{H}})_L$ and $(C_{\mathrm{H}})_l$. Using the method of Puls

$$(C_{\mathrm{H}})_{L,l} = \left(C^{\mathrm{S}}_{\mathrm{H}}\right)_{L,l} \times \exp\left\{\frac{(\bar{w}^{\mathrm{inc}}_t)^{\mathrm{eff}}_{L,l} + (\overline{w}^{\mathrm{a}}_t)_{L,l}}{xRT}\right\}\exp\left\{\frac{(\overline{w}^{\mathrm{a}}_{\mathrm{H}})_{L,l}}{RT}\right\}, \tag{A.15}$$

where $C^{\mathrm{S}}_{\mathrm{H}}$ is the concentration of hydrogen in equilibrium with unconstrained hydrides when there is no external stress $= C_0\exp(-Q_{C_{\mathrm{H}}}/RT)$, $(\overline{w}^{\mathrm{inc}}_t)^{\mathrm{eff}}$ total effective molal strain energy in an infinite matrix and the hydride precipitate, $(\overline{w}^{\mathrm{a}}_t)$ the interaction energy of the hydride with the applied stress $= -\overline{V}_{\mathrm{hydride}}\sigma^{\mathrm{a}}_{i,j} \cdot \varepsilon^T_{i,j}$ and $\overline{V}_{\mathrm{hydride}}$ is the molal volume of hydride.

References

[1] R. Dutton, M.P. Plus, in: A. Thompson, I.M. Bernstein (Eds.), Effects of Hydrogen on Behaviour of Materials Metallurgical Society, AIME, New York, 1976, p. 526.
[2] R. Dutton, M.P. Puls, in: Conference on Effect of Hydrogen on Behaviour of Materials, American Institute of Mining, Metallurgical, and Petroleum Engineers, 7–11 September 1975, p. 516.
[3] M.P. Puls, Metall. Trans. A 21 (1990) 2905.
[4] J.L. Waisman, G. Sines, L.B. Robinson, Metall. Trans. 4 (1973) 291.
[5] A. Sawatzky, J. Nucl. Mater. (1960) 62.
[6] C.E. Coleman, J.F.R. Ambler, Can. Metall. Quart. 17 (1978) 81.
[7] A. Sawatzky, J. Nucl. Mater. 2 (4) (1960) 321.
[8] G.J.C. Carpenter, J. Nucl. Mater. 48 (1973) 264.
[9] M.P. Puls, Acta Met. 32 (8) (1984) 1259.
[10] C.E. Coleman, J.F.R. Ambler, ASTM STP 633 (1977) 589.
[11] J.F.R. Ambler, in: D.G. Franklin, R.B. Adamson (Eds.), Zirconium in the Nuclear Industry, ASTM STP 824, American Society for Testing and Materials, PA, 1984, p. 653.
[12] S. Sagat, J.F.R. Ambler, C.E. Coleman, Application of acoustic emission to hydride cracking, Atomic Energy of Canada Limited Report, AECL-9258, 1986.
[13] A.A. Mason, Metal temperatures and thermal stresses near leaking Bruce-2 pressure tube cracks, AECL Report no. CRNL-2571, July 1983.
[14] W.N. Selander, P.Y. Wong, P.Z. Rosta, Thermal performance of pickering – a fuel channels before and after pressure tube to calandria tube contacts, Atomic Energy of Canada Ltd., Report no. CRNL-02439, December 1982.
[15] S. Sagat, C.E. Coleman, M. Griffiths, B.J.S Wilkins, in: A.M. Garde, E.R. Bradley (Eds.), Zirconium in the Nuclear Industry: Tenth International Symposium, ASTM STP 1245, American Society for Testing and Materials, PA, 1994, p. 35.

[16] C.E. Coleman, L.A. Simpson, Evaluation of a leaking crack in an irradiated CANDU pressure tube, fracture mechanics verification by large-scale testing, EGF/ESIS8, in: K. Kusmaul (Ed.), Mechanical Engineering Publications, London; Atomic Energy of Canada Limited Report, AECL 10246, 1991, pp. 189–201.

[17] G.D. Moan, S. Sagat, P.J. Ellis, J.K. Mistry, P.J. Richinson, D.K. Rodgers, C.E. Coleman, Leak-before-break in CANDU pressure tubes, Recent Advances, 1993 ASME Pressure Vessels and Piping Conference, Denver, Colorado, July 1993, pp. 25–29.